A simple method for the assessment of the Contact Modulus for coated systems

S J Bull

School of Chemical Engineering and Advanced Materials,

Newcastle University,

Merz Court,

Newcastle upon Tyne,

NE1 7RU,

UK.

e-mail: steve.bull@ncl.ac.uk

Abstract

This paper describes a simple method to determine the elastic modulus of a coating on a substrate using nanoindentation based on the load support of a truncated cone of material beneath the indenter. The cone angle is shown to be 32.48^{o} in all cases. The effect of the coating on the measured contact modulus increases more rapidly as the contact scale is reduced. The model describes the behaviour of a range of coating substrate systems very well but deviations are observed in cases where pile-up or tip end-shape variations affect the experimental data. It is possible to use a fit of a simplified form of the model to experimental data for coatings on stiff substrates to determine the elastic properties of the coating independent of the substrate. The model can be generalised for multilayer coatings; this is essential when compliant coating layers are sandwiched between stiffer layers. The model shows that the mechanical properties of thin stiff coatings on compliant substrates cannot be successfully determined from indentation data. The ISO 14577 extrapolation method should therefore not be used in such circumstances.

Keywords

Nanoindentation, coating, elastic properties, Young's Modulus

1. Introduction

Nanoindentation has been widely used to determine the surface mechanical properties of bulk materials and coatings. In this technique a continuous record of indenter load and displacement is taken as an indenter of known shape is pressed into and removed from a sample surface. If the indenter is sharp enough (and the applied load high enough) plastic deformation will occur leaving a permanent impression, the size of which is related to the plasticity properties of the material. The surface will also flex elastically and thus the measured indenter displacement contains both elastic and plastic contributions. The slope of the unloading curve (unloading stiffness) is related to the

elasticity of the sample. The Oliver and Pharr analysis method [1] for extracting mechanical property data from load displacement curves determines the elastic deflection of the surface at the edge of the contact using the unloading stiffness and from this the contact depth which is the depth of the impression before any elastic recovery in its shape occurs on unloading. Given this the hardness and contact modulus of the sample can be calculated if the indenter shape is accurately known.

In nanoindentation testing of a coating/substrate system the normal analysis method of Oliver and Pharr [1] has been assumed to give a reasonable value for coating properties if the penetration depth is low enough (typically less than 10% of coating thickness [2]). Whereas there is some validity in this for hardness values the contact modulus data may not be amenable to the same analysis. The ISO14577 standard recommends extrapolating a plot of hardness or contact modulus against contact depth to zero depth to obtain coating properties. Whereas this produces reasonable values for coatings on hard stiff substrates the values determined in this manner for stiff coatings on compliant substrates can be greatly underestimated.

In fact it is questionable whether it is possible to determine the elastic properties of a coating independent of the substrate by direct measurement even with such an extrapolation approach. The coating and substrate beneath an indenter are effectively two springs in series and thus there will always be a substrate contribution in the contact modulus data measured from them. Therefore a modelling approach is necessary to extra the coating properties from the data obtained. This paper outlines a simple approach whereby this may be achieved and illustrates the results for aluminium oxide coatings on hard, stiff (glass) and compliant (PET) substrates.

The first attempt to describe the variation of measured elastic modulus with contact depth for a coated system was introduced by Doerner and Nix who developed an empirical function containing exponential terms based on test data for tungsten films on silicon [3]. This expression was generalised by King [4] using numerical methods. In both cases a weighting factor was used to determine the contributions of coating and substrate at each value of a/t where a is the radius of the contact patch and t is the coating thickness. Bhattacharya and Nix [5] used finite element analysis to show good agreement of the model with results for aluminium on silicon which supported the work of King. More complex formulations have been developed based on the work of Gao et al [6] who derived an analytic function for the combined modulus of the film/substrate system which did not include any empirical parameters. Rar et al [7] recently extended this approach to be valid at a large range of contact conditions and found that a good fit with experimental data could be achieved if the film thickness was replaced by the film thickness minus the contact depth in the Gao equations. A major disadvantage of these approaches is that they were originally formulated in terms of the shear modulus, G, and the Poisson's ratio is needed for determining Young's Modulus and contact modulus from the expression. An alternative formulation was developed by Bec at al [8] based on considering the coating and substrate as two springs in series and working out an effective contact compliance based on this assumption using correcting polynomial functions of the form $f(a)=1+ka^n$ where k and n are constants. These approaches have been compared in the paper by Bec [9]. Most of these models show reasonable agreement with experimental data at small deformations but the agreement at larger deformations and where the modulus mismatch is large is not so good, probably because membrane stresses in the film are ignored.

Korsunsky and Constantinescu [10] recently considered the same problem in terms of indenter geometry and suggested that another parameter which needs to be considered is the ratio of the indenter radius to the coating thickness. For very sharp indenters it is possible to recover the properties of the coating with low load indentations but this is no longer true as the indenter radius increases close to the flat punch analyses discussed in the previous paragraph. They defined a model response function which fitted their experimental results which is very similar to a formulation previously developed for coating hardness [11]; this type of model shows a transition from the properties of the coating at low indentation depth to those of the substrate at high indentation depth with a different form of weighting function to the earlier works in the mid range.

In this paper an alternative simple formulation is developed that uses no adjustable parameters and can be applied to single and multiple layer coatings. It is similar to the other analytical models in that the moduli of the coating and substrate are combined via weighting functions which vary as the contact scale changes. However, these weighting functions are developed from the assumption that the indentation load is supported by a conical region of elastic deformation below the contact.

2. The model

Assume that an indenter is loaded onto the surface of the coating with contact radius a_0. At the surface the load is supported by a contact area $A=\pi a_0^2$ but the area of load support is increased as we consider layers in the coating and substrate below the surface. If we consider the material divided up into a number of layers parallel to the surface then the load on the contact area of the top surface is transferred to a slightly larger area on the next layer below and so-on throughout the coating and substrate thickness. As the area increases the contact stress decreases and, assuming elastic behaviour, the strain in each successive layer is reduced. Thus the displacement of the material due to the loaded indenter is greatest just beneath it and falls away as the distance from the indenter tip increases. Given this observation it should be possible to measure the contribution of the coating to the overall displacement and hence the modulus of the coating if the expression for the change in loaded area with depth is known.

Let us assume that there is a linear increase in the area supporting the load as we go deeper into that material; this effectively gives us a truncated cone for the loaded volume, seen in cross section in Figure 1.

If we assume a totally rigid indenter then the indenter displacement, δ, is give by the sum of all the displacements in the individual layers beneath the indenter. In an individual layer

$$d\partial = \frac{Pdx}{EA} \tag{1}$$

Where P is the load applied to the indenter, E is the Young's Modulus of the layer and A is the contact area at a given depth x. If the semi-angle of the cone is α then

$$A = \pi(a_0 + xtan\alpha)^2 \tag{2}$$

Combining (1) and (2) we have in the coating

$$d\partial = \frac{P}{E_c}\frac{dx}{\pi(a_0+xtan\alpha)^2} \tag{3}$$

where E_c is the Young's Modulus of the coating. This can be integrated through the coating thickness to give the total indenter displacement due to elastic deformation of the coating. Thus

$$\partial_c = \frac{P}{\pi E_c}\int_0^{t_c}\frac{dx}{(a_0+xtan\alpha)^2} \quad (4)$$

Where t_c is the coating thickness. Integrating gives

$$\partial_c = \frac{P}{\pi E_c}\left[\frac{1}{a_0 tan\alpha} - \frac{1}{a_0 tan\alpha + t_c tan^2\alpha}\right] \quad (5)$$

By a similar approach integrating through the substrate thickness we have

$$\partial_s = \frac{P}{\pi E_s}\left[\frac{1}{a_0 tan\alpha + t_c tan^2\alpha} - \frac{1}{a_0 tan\alpha + (t_c+t_s) tan^2\alpha}\right] \quad (6)$$

where E_s is the Young's Modulus of the substrate and t_s the substrate thickness. The total indenter displacement is then

$$\partial = \partial_c + \partial_s \quad (7)$$

Both the displacements in the coating and substrate are a linear function of contact load and thus the unloading stiffness S=P/∂. Given that for a flat punch S=2Ea [12] it is possible to calculate the effective Young's Modulus of the coating/substrate system

$$E = \frac{P}{2a_0(\partial_c+\partial_s)} \quad (8)$$

For a deformable indenter E must be replaced by E*, the contact modulus, given by

$$\frac{1}{E^*} = \frac{1-\nu_1^2}{E_1} + \frac{1-\nu_2^2}{E_2} \quad (9)$$

where the subscripts 1 and 2 refer to the properties of the sample and indenter respectively, ν is Poisson's ratio and *E* is Young's Modulus. In this study the diamond indenter properties are E=1141GPa and v=0.08.

The contact radius can be related to the contact depth, h_c, determined by the Oliver and Pharr method [1], if the indenter geometry is known. For a Berkovich indenter,

$$h_c = \sqrt{(\pi/k)}\, a_0 \quad (10)$$

where k=24.5. This assumes a perfect tip which is reasonable at larger contact areas corresponding to higher load tests. When comparing with experimental data it should be recognised that the experimental contact depth will have been used to determine a contact area through a measured tip area function – thus for a given contact depth there could be a range of contact moduli depending on the area function; usually lower values are measured for a blunter tip. To avoid this problem the contact radius can be determined from the contact area, A, determined from the contact depth using the tip area function, via

$$a_0 = \sqrt{A/\pi} \quad (11)$$

Or more conveniently from the load and measured hardness

$$a_0 = \sqrt{\frac{P}{\pi H}} \tag{12}$$

2.1 What is the angle alpha?

Since the indentation of a bulk material is almost identical to that of a coating with large thickness equation (5) can be applied to a bulk material of known elastic properties to determine the truncated cone angle α. If we assume that the material thickness is very much greater than the contact radius the second term in the brackets in equation (5) goes to zero and

$$\partial = \frac{P}{E\pi a_0 tan\alpha} \tag{13}$$

The unloading stiffness is P/∂ and using the Sneddon approximation [12]

$$S = E\pi a_0 tan\alpha = 2Ea_0 \tag{14}$$

Thus $tan\alpha$=2/π and α=32.48^o. This angle is independent of the choice of material and the properties of coating or substrate. Since the geometry of the stress field below the indenter does not change with size if the indenter is self similar then α should be independent of indent size, though it may change at small scales if the self-similarity is broken e.g. by tip blunting. This is not an issue in this study since sharp tips have been used and data has been obtained for contact depths much greater than the tip defect.

Combining equations (5), (6) and (8) with this expression for $tan\alpha$ it can easily be shown that:

$$E = \frac{1}{\frac{1}{E_C}\left[1-\frac{\pi a_0}{\pi a_0+2t_C}\right]+\frac{1}{E_S}\left[\frac{\pi a_0}{\pi a_0+2t_C}-\frac{\pi a_0}{\pi a_0+2(t_C+t_S)}\right]} \tag{15}$$

From this formulation it is clear that as a_0 tends to zero the value of E tends to E_c and that if a_0 is very much greater than t_c and t_s is much greater than a_0 then E tends to E_s as might be expected.

2.2 Model Predictions

By plotting the output of equation (15) against contact radius for a number of different coating substrate systems it is possible to determine the effect of coating/substrate modulus mismatch and coating thickness Figure 2 shows the variation of contact modulus with contact depth (determined from contact radius using equation (10)) for a thin stiff coating on glass (t_c=150nm, E_c=140GPa, E_s=70GPa). A minimum contact radius of 10nm is used for all calculations in this study which corresponds to the lowest contact depth (~4nm) which is practically measurable with the best indenters after intensive tip calibration. As the contact depth is reduced the predicted contact modulus increases and this increase becomes more rapid at small scales. However, even at the smallest contact radius used in the calculations the predicted modulus is less than the coating modulus as some contribution from substrate elasticity is present. When using the ISO14577 method for assessing the modulus of the coating (i.e. a linear extrapolation of the data to zero contact depth) it is clear that to get a value which approximates the input coating modulus only the very lowest contact radius data points should be used in the extrapolation. If the first four data points here are used an extrapolated modulus of 133GPa is produced (a 5% error) and the value is reduced as more data points are included. In fact to get a reasonable extrapolated value it is

necessary to only use data points for fitting where the contact depth is less than ~10% of the coating thickness. The challenge is to get reliable experimental data in this contact depth range.

The effect of coating stiffness is shown in Figure 3a for 150nm coatings on glass. The bigger the modulus mismatch with the glass substrate the bigger the difference observed at low contact radius. Even when the contact radius is two or three times the coating thickness there is a substantial difference between the contact modulus of the coating/substrate system and that of the substrate. The contact radius must be much smaller than the coating thickness if reliable extrapolation is to be achieved. The effect is more dramatic if the contact modulus of the coating is fixed and that of the substrate varied as is illustrated for 800nm copper coatings in Figure 3b. When the substrate is stiffer the contact radius must be more than the coating thickness for substrate properties to be measured. However, as the substrate stiffness is reduced the deviation from substrate stiffness occurs at lower and lower contact radius values and measuring the coating properties becomes increasingly difficult.

As coating thickness increases its effect on the contact modulus of the coating/substrate system increases (Figure 4a). However, if the contact radius is normalised by the coating thickness, the data collapse onto a single curve (Figure 4b). The ISO14577 extrapolation technique gives reasonable data when $a/t<0.17$ which corresponds to $h_c/t<0.06$ for a perfect tip. Slight errors in the coating thickness lead to a deviation in the modulus vs contact depth curve from this ideal behaviour but extrapolation to zero depth at low depths generates the same coating modulus within experimental error.

2.3 Model validation

The commercial finite element program ANSYS 9.0 was used in this study to mimic the nanoindentation process. A deformable–deformable contact pair and the Augmented Lagrangean method were chosen in this model. A halfsymmetry model was adopted to save computing time and roller boundary conditions were applied on the centre line and bottom line. The interface between the indenter and the specimen was assumed to be frictionless. A rigid conical tip with half angle 70.3^{o} and a 20nm radius spherical cap was used for the indenter. A 2-D 8-Node element was selected to model the specimen [13]. Mesh refinement in the region of the contact was used to ensure accuracy and convergence of the solutions as previously published [2]. Finite element simulations where a rigid conical indenter was pressed into a coated surface with a plane stress modulus of 120GPa for the substrate and 240GPa for the coating (and vice versa) have been performed to compare with the analytical model outputs. The yield stresses of the coating and substrate were set to 4GPa and the load displacement curves obtained at a range of peak loads. The contact radius, a_0, was determined from the deformed shape under 95% unload and the contact modulus was determined from the unloading curve using equation (14). The contact radius was normalised by the coating thickness (2μm in this case). The variation in modulus with a/t is very similar to the results reported by Bec et al [9] showing that the FE simulation method is reasonable.

Predictions from equation (14) are compared with the results from FE simulations in Figure 5; the plain strain moduli were used for the contact moduli of the layers in equation (14). Reasonable fits between model and experimental data were observed in both cases. When the coating is stiffer than the substrate the fit is good at low and high values of a/t but is less good at intermediate ranges

(Figure 5a). In the case that the coating is less stiff than the substrate the fit is much better across the complete range of a/t (Figure 5b). In both cases the model predictions are almost identical to the predictions from the model of Bec et al [9], the only differences arising because the Bec et al model does not consider the effect of the substrate thickness on predicted contact modulus.

Equation 14 can be fitted to the FE data to determine the coating and substrate moduli. In the case of the data in Figure 5a the fitted values of E_c and E_s are 242GPa and 106GPa respectively whereas the values from the data in Figure 5b are 118GPa and 186GPa respectively. It can be clearly seen that the error in the fitted values for the coating contact modulus is very small (less than 2% in both cases) with the stiffer coating giving slightly better results. The data for the substrate stiffnesses show greater errors, 12% for the stiff coating on the compliant substrate and 23% for the compliant coating on the stiffer substrate. This is not surprising because the shape of the stress distribution below the surface is not conical and the deviations from this will increase below the surface. However, the good values for the fitted coating properties show that this is a reasonable approach to determine coating properties from coating/substrate system data.

3. Experimental validation

3.1 Coating/substrate systems investigated

In all the experiments carried out in this study coatings were deposited on very low roughness substrates and were sufficiently thin that the roughness of the coating was not significantly different from that of the substrate; Ra values are indicated in the figure captions for those samples from which experimental data was obtained. Given the values measured the effect of roughness on measured indentation data is expected to be minimal.

Two micron thick TiN coatings (E=600GPa from acoustic measurements) were deposited onto 5mm thick polished stainless steel (E=210GPa) by sputter ion plating. One micron copper coatings (E=120GPa) were deposited on 1mm thick sapphire (E=440GPa) and 0.1mm thick Polyimide (E=5GPa) by electron beam evaporation. The substrate modulus values in parentheses were determined from nanoindentation measurements on the uncoated substrate (corrected for pile-up in the case of the stainless steel substrate using AFM images of the impressions created). The deposition temperature was 100^{o}C and the deposition rate was 1nm/s. 800nm copper layers were also deposited on a thermally oxidised 0.38mm thick (100) silicon wafer for comparison (for silicon E=167GPa from nanoindentation measurements). In this case a 1 micron thick silica layer separated the copper from the silicon. Amorphous aluminium oxide samples were deposited on soda lime silica glass (E=70GPa) and PET (E=5GPa) by atomic layer deposition using trimethyl aluminium and water vapour in alternate cycles. Coatings were deposited at 150^{o}C and 80^{o}C. The nominal coating thickness was determined by ellipsometry on silicon samples deposited at the same time and was 150nm at the lower temperature at 160nm at 150^{o}C. Despite the fact that all coatings were deposited in the same deposition run at each deposition temperature, ion beam analysis revealed that the coatings on PET were about 40% thicker than the coatings on glass and scanning electron microscopy of fractured cross sections showed that the thickness on glass was the same as the ellipsometry value.

3.2 Nanoindentation testing

Coated samples were attached to a heavy steel block using cyanoacrylate adhesive prior to testing to minimise support compliance issues. Nanoindentation testing on hard coating/substrate systems was performed on a Nanoindenter 2 fitted with a general purpose Berkovich tip (tip end radius 250nm) at peak loads from 1mN to 500mN. No peak load hold was used but a hold at 70% unload was used for thermal drift correction. Tests were performed in continuous stiffness mode (proportional loading $dP/P=0.05s^{-1}$, oscillation frequency 45Hz, amplitude 2nm). Nanoindentation testing on the soft/compliant coating/substrate systems was performed on a Hysitron Troboindenter fitted with a new Berkovich diamond (average tip end radius 59nm determined from elastic indentations in fused silica). Indentation tests were performed under displacement control with a loading and withdrawal rate of 500nm/s and a 4s peak load hold to allow for creep run out. A 40s 2μN contact load hold prior to the test was used for thermal drift correction. Indentations were produced at a range of peak displacements from 3 to 400nm depending on the sample.

In both cases hardness and contact modulus data were determined from the load displacement curves by the method of Oliver and Pharr [1]. Tip end-shape calibration was performed using a fused silica standard prior to testing using the approach outlined by Oliver and Pharr.

4. Results

In the case where the properties of the coating and substrate are well known equation (15) can be used to predict the elastic response of the coating/substrate system. The following subsections consider different types of coating/substrate system.

4.1 Stiffer Coating on a stiff substrate

Depending on the indentation system and software configuration used for nanoindentation elastic data may be output in terms of Young's Modulus (with an assumption about the Poisson's ratio of the system) or contact modulus. Figure 6 shows the variation of Young's Modulus with depth for TiN coated steel determined using a Nanoindenter 2 in continuous stiffness mode compared with predictions from equation (15) using thickness data obtained from ball cratering and contact moduli for coating and substrate obtained from unloading curve analysis using the method of Oliver and Pharr [1]. A Poisson's ratio of 0.28 was used to calculate the Young's Modulus from the measured contact modulus. The slight reduction in modulus at the lowest contact depths in the experimental data is due to the fact that this is the region where the elastic to plastic transition is occurring and the Oliver and Pharr analysis cannot be used to obtain reliable contact modulus data. The deviation from the model between 100nm and 300nm contact depth is due to blunting of the tip – the tip calibration was carried out some time before the coated sample was measured and changed whilst indenting other materials before testing the hard TiN coating. The ISO14577 extrapolated value for the Young's Modulus of TiN is typically about 550GPa (contact modulus 388GPa) whereas acoustic wave velocity measurements generally give Young's Modulus values around 600GPa which gives a contact modulus of 415GPa. Correcting the acoustic value for the TiN coating by including the substrate contribution in equation (15) produces a predicted curve which is a good match with experimental data and an extrapolated Young's Modulus close to the usually measured value for TiN in nanoindentation tests on thicker coatings.

4.2 Stiff coating on a stiffer or more compliant substrate

Figure 7 shows a comparison of the predictions of contact modulus as a function of relative indentation depth (i.e. contact depth normalised by coating thickness) against measured data for the one micron thick copper coating on sapphire and polyimide. There is an excellent agreement between predictions and experimental data for the polyimide substrate and a good agreement for copper on sapphire when the RID is less than 0.6. At higher RID for the sapphire substrate there is considerable pile up of copper around the indentation and the contact modulus determined by the method of Oliver and Pharr is overestimated leading to the deviations observed here. It is interesting to note that for the low modulus polyimide substrate the measured contact modulus does not approach that of the coating even at the lowest practical contact scale for measurement. Using the ISO14577 extrapolation approach will predict a coating contact modulus about half the bulk value since the elastic deformation of the coating/substrate system is dominated by the substrate. In this case the simple conversion of contact radius to contact depth using equation (10) was acceptable as most of the data was obtained at contact depths where the deviation from ideal indenter geometry was small.

4.3 Stiff coating on a compliant or very compliant substrate

For the thinner ALD alumina coatings the tip defect is much more critical and hence for comparison with experimental data the experimental contact area, A_c, calculated from the contact depth and corrected by the tip area function was converted to a contact radius, a, via $A_c=\pi a^2$. Comparisons with experimental data were made in terms of both contact radius (Figure 8a, c) and contact depth (Figure 8b, d). In this case the properties of the coating were not known prior to testing. Since the coatings on the stiffer glass substrate are more likely to be amenable to the ISO14577 extrapolation analysis this was used to identify the correct coating elastic modulus. Predictions were then made about the behaviour on the more compliant substrate – since this was coated at the same time the mechanical response of the coating was expected to be similar.

The coating contact modulus (E_c=160GPa) determined for the coatings on glass (E_s=70GPa) is the same whether or not the contact radius (Figure 8a) or contact depth (Figure 8b) is used in the prediction process and agrees with values measured from coatings on other stiff substrates when deposited by the same method. In the range of contact conditions investigated the fit with predictions is best at low penetration depth an d, after some deviation, improves as the contact radius or depth increases (as seen in the comparison between model and FE data in Figure 5a). The deviations are probably due to a combination of model accuracy and the rounding of the tip.

The coatings on the compliant PET substrate show much lower measured contact moduli across the complete range of contact depths. In this case the coating data used to model the coatings on glass was used to predict the behaviour of the coatings on the more compliant PET substrate (E_s=4GPa). The agreement with experiment is good whether expressed in terms of contact radius (Figure 8c) or contact depth (Figure 8d). Extrapolation of the low penetration data to zero depth following the ISO14577 approach will seriously underestimate the modulus of the coating.

4.4 Stiff coating on a stiff substrate with a less stiff intermediate layer

Equations (5)-(8) can easily be modified for a coating with two or more layers. In the case of a copper layer on a silica intermediate layer on silicon equation (5) remains valid for the coating contribution but, for an interlayer of thickness t_i and modulus E_i, equation (6) becomes

$$\partial_i = \frac{P}{\pi E_i}\left[\frac{1}{a_0 tan\alpha + t_c tan^2\alpha} - \frac{1}{a_0 tan\alpha + (t_c+t_i) tan^2\alpha}\right] \quad (16)$$

And for the substrate

$$\partial_s = \frac{P}{\pi E_s}\left[\frac{1}{a_0 tan\alpha + (t_c+t_i) tan^2\alpha} - \frac{1}{a_0 tan\alpha + (t_c+t_i+t_s) tan^2\alpha}\right] \quad (17)$$

In equations (7) and (8) $\partial_c+\partial_s$ is replaced by $\partial_c+\partial_i+\partial_s$. Predictions for this bilayer model and the single layer model for 800nm copper on silicon with a 1micron intermediate silica layer are shown in Figure 9 compared to experimental data. Initially the experimental data appear to follow the curve for the single layer prediction but as the contact scale increases the predicted contact modulus from the bilayer model and the experimentally measured values decrease as contact depth increases whereas the single layer model shows an increase as expected from a coating on a stiffer substrate. Since the system acts as a series of springs in series where the reciprocals of the spring constants are added to get the effective spring constant the lowest Modulus layer dominates behaviour if it not too far below the contact surface. The fit for the bilayer model to experimental data is very good – at the loads used to test this sample the effect of pile-up is only marginal.

5. Discussion

The simple analytical expressions developed in this study show a remarkable ability to predict the variation of contact modulus with contact depth in a range of coated systems. The simple linear expansion of the load supporting area appears to work in all the systems tested here. It should be noted that the idea of a cone of load support has been previously suggested as the way to determine the stresses and deflections around the contact in a bolted joint where the cone angle was 45^o [14]. However, there was no theoretical justification for this angle as is provided in this paper. Comparing a truncated cone contact radius a_0 and cone angle 32.48^o with the stress distribution below an elastic impression from a conical indenter (Figure 10) shows that the majority of the compressive deformation is contained within the truncated cone so the geometry seems to be a reasonable choice but it may be possible to refine the analysis with a form of the load supporting volume which more closely matches the stress distribution. However, given the simplicity of this analysis and the agreement with experimental data this may be unnecessary.

There is nothing in the model that depends on the geometry of the impression; rather it is assumed that the contact patch remains parallel to the original surface. This is likely to be a reasonable approximation at low loads for blunt indenters as are usually used in indentation testing but will no longer be valid for sharp contacts where excessive plastic deformation can locally thin the coating

In comparison with experimental data results are generally very good if the correct coating thickness is used in the model. In fact an originally poor fit for the ALD alumina on glass let to a more careful measurement of the coating thickness used in the modelling which led to much better agreement. Experimental data affected by pile-up and tip defects will deviate from the model at high and low

loads respectively. The former is a particular issue when testing metal coatings on hard substrates such as silicon or sapphire. When materials show appreciable creep the contact area can increase compared to the value determined by the Oliver and Pharr analysis either during loading or during high load holding periods and the pile-up geometry will be affected. In this case the contact radius and contact modulus for use in modelling should be obtained from experimental measurements of the contact area if reliable results are to be generated.

Using the ISO14577 extrapolation method gives good values for the coating contact modulus for coatings on a hard, stiff substrate but the extrapolated modulus drops as the coating thickness is reduced (Figure 11) or the substrate modulus is reduced (Figure 12). This is because it is impossible to measure contact modulus data at sufficiently low contact depth when the deformation is dominated by substrate elasticity. For accurate measurements of coating modulus a coating thickness of at least one micron is required. For good extrapolation some experimental data where $a/t<0.01$ is required which can be very difficult to achieve experimentally, particularly if compliant substrates are used.

The simplicity of the model leads to a direct fitting approach if equation (15) can be simplified further. If we assume that the substrate is very much thicker than the coating ($t_s>>t_c$) then the last term on the denominator of equation (15) will tend to zero and can be ignored. Equation (15) can then be rewritten

$$E = \frac{1}{\frac{1}{E_C}\left[\frac{2t_C}{\pi a_0+2t_C}\right]+\frac{1}{E_S}\left[\frac{\pi a_0}{\pi a_0+2t_C}\right]} \quad (18)$$

where the terms are as defined previously. Equation (18) may be fitted to a plot of E vs a_0 to determine the coating and substrate modulus and the coating thickness. If data is available in terms of contact depth, δ_c, then the same equation can be used but the constant π will change and can be a fitting variable. The fit can be further simplified if the substrate properties and coating thickness are available from other sources. In fact equation (18) can be derived by rearranging the expression derived by Bec et al in [9] to predict the contact modulus of a coated system as a function of contact scale further confirming the validity of the approach developed here.

This fitting approach has been applied to the experimental data for TiN coated steel in Figure 6 and delivers values for coating modulus (540±67GPa) and coating thickness (2.0±0.1μm) which are in very good agreement with other measurements. The errors in the fit are reasonable as there is sufficient data at low contact depth. The fitted value of substrate modulus is very low again showing that the model deviates from experiment as the distance below the surface increases.

The fitting approach has also been applied to the 150nm ALD alumina coatings in Figure 8 giving the data in Table 1. The fit is reasonable for the coating properties on the glass substrate giving very similar values for the coating and substrate moduli depending on whether the fit is in terms of contact radii or contact depth. However, the errors in the fitted values are much larger than in the case of a thicker coating on a stiffer substrate, in this case more than 25% for coating modulus. The quality of the fit on the PET is much poorer and it is difficult to get the fit to converge. The fitted coating modulus is much lower than expected and the error in the fit is almost as large as the value determined. However, the fitted substrate properties are good with relatively low errors (<20%) indicating that the substrate dominates the measured data as expected.

Work by Korsunsky and Constantinescu [10] has shown that the contact modulus of a coated system measured by indentation does not converge to the coating value at low penetration unless the radius of the indenter is less than 10% of the coating thickness. Despite the fact that a new sharp Berkovich indenter was used in this work this criterion has not been met since the ratio of tip radius to coating thickness is ~0.4. In addition, the data obtained at low penetration depths is significantly affected by tip calibration issues (Figure 13) and many indentations do not show plastic deformation so there is a lack of data to use in the fit. This indicates that a curve fitting approach will not produce reliable coating data for very thin stiff coatings on compliant substrates. In this case a fit of equation (18) cast in terms of contact depth will not converge easily and gives exceptionally high values of contact modulus which are not physically reasonable. This approach to fitting should not therefore be used.

In cases where fitting cannot be used equation (15) can still be used to predict the variation of contact modulus with contact radius for comparison with experimental data and this can be used to check the consistency of data obtained from other methods with that from indentation. With most practical indenters a coating thickness of at least 3μm is required to ensure that a good value for coating modulus can be extracted by a fit using equation (18).

6. Conclusions

A simple analytic model has been developed to predict the variation of contact modulus with contact radius (or depth) for a single or double layer coating on a substrate. The model shows excellent agreement with experimental data for a stiff coating on a less stiff substrate whether the substrate has high or low stiffness. Agreement is also good for a less stiff coating on a stiffer substrate. It is important that all layers in the coating stack are included in any predictive model if the behaviour is to be fully understood – the approach has been demonstrated for one or two coating layers here but can easily be generalised for any multilayer coating stack.

Care should be taken when using extrapolation techniques to determine the elastic properties of the coating. For coatings on a stiff substrate the extrapolation approach is valid but accurate data is only produced in cases where the contact modulus of the coating is similar to that of the substrate. For stiff coatings on very compliant substrates it is almost impossible to measure coating properties by extrapolation and a modelling approach as outlined here is essential. However, fitting the model here to experimental data cannot generally give reliable data for coatings on very complaint substrates unless they are thick enough that sufficient data can be generated at low penetration depths.

Acknowledgements

The author would like to thank the Royal Academy of Engineering and the Leverhulme Trust for provision of a Senior Research Fellowship which allowed him to complete this work.

References

[1] W.C. Oliver and G.M. Pharr, J. Mater. Res., **7** (1992) 1564.

[2] J. Chen and S.J. Bull, Vacuum, **83** (2009) 911.

[3] M.F. Doerner and W.D. Nix, J. Mater. Res., **1** (1986) 601.

[4] R.B. King, Int. J. Solids Struct., **23** (1987) 1657.

[5] A.K. Battacharya and W.D. Nix, Int. J. Solids Struct., **24** (1988) 1287.

[6] H. Gao, C.H. Chiu and J. Lee, Int. J. Solids Struct., **29** (1992) 2471.

[7] A. Rar, H. Song and G.M. Pharr , Mat. Res. Soc. Symp. Proc., **695** (2002) 431.

[8] S. Bec, A. Tonck, J.M. Georges, E. Georges and J.L. Loubet, Phil. Mag., **A74** (1996) 1061.

[9] S. Bec, A. Tonck and J.L. Loubet, Phil. Mag., **86** (2006) 5347.

[10] A.M. Korsunsky and A. Constantinescu, Thin Solid Films, **517** (2009) 4835.

[11] A.M. Korsunsky, M. R. McGurk, S.J. Bull and T.F. Page, Surf. Coat. Technol., **99** (1998) 171.

[12] I.N. Sneddon, Int. J. Eng. Sci., **3** (1965) 47.

[13] ANSYS 9.0 Documentation, ANSYS Inc (2009).

[14] J.E. Shigley, Mechanical Engineering Design, McGraw-Hill, New York, 1986, pp305-307.

Tables

Table 1 Fitted properties for ALD alumina coatings on glass and PET using equation (18).

Substrate	Property	From E vs a_0	From E vs δ_c	From another technique
Glass	E_c (GPa)	165±49	160±42	160 – ISO14577
	t_c (nm)	205±55	106±36	150 – Ellipsometry
	E_s (GPa)	58±9	67±12	65 – nanoindentation on uncoated glass
PET	E_c (GPa)	85±75	767±614	160 – bending tests
	t_c (nm)	214±120	338±156	210 – Ellipsometry
	E_s (GPa)	3.9±0.5	3.3±0.6	4 – tensile testing

Figures

Figure 1: Cross sectional view of model geometry.

Figure 2: Variation of E with contact depth for a 150nm stiff coating (E=140GPa) on glass (E=70GPa).

Figure 3: (a) Variation of E with contact radius for 150nm coatings with a range of elastic moduli on glass (E=70GPa). (b) Variation of E with contact radius for 800nm copper (E_c=120GPa) on various substrates.

Figure 4: Variation of E with (a) contact radius, a, and (b) a/t for a stiff coating (E=140GPa) on glass (E=70GPa).

Figure 5: Comparison of model and FE predictions for coatings on different substrates, (a) $E_c=2E_s$ (E_s=120GPa) and (b) $E_c=0.5E_s$ (E_c=120GPa). The predictions from the model developed here and those from the model developed by Bec et al [9] are almost identical and match the FE data very well.

Figure 6: Young's modulus of TiN on stainless steel (Ra=30nm). Predictions from equation (15) using measured stiffness data and thicknesses are compared to experimental data and a fit of equation (15) to the experimental data. Coating properties are very consistent in both cases.

Figure 7: Contact modulus of 1μm copper on sapphire (Ra=5nm) and polyimide (Ra=20nm) as a function of contact scale.

Figure 8: Contact modulus vs contact radius (a), (c) and contact depth (b), (d) for ALD alumina on glass (Ra~0.5nm) and PET (Ra~0.4nm) deposited at (a), (b) 80^{o}C and (c), (d) 150^{o}C. Coating properties determined in (a) and (b) are used for the predictions in (c) and (d).

Figure 9: Contact modulus vs depth for 800nm copper on silicon (Ra=0.2nm) with a 1 micron silica intermediate layer. Predicted behaviour with and without the silica layer shows the importance of the silica in controlling behaviour.

Figure 10: Comparison of the truncated cone geometry with the stress field under a conical indenter.

Figure 11: Variation of the ratio of extrapolated contact modulus with coating thickness for two different coating/substrate compliance ratios. The stiff coating only gives accurate data when its thickness is greater than 1μm whereas accurate values for the contact modulus of the compliant coating can be determined down to a thickness of 100nm.

Figure 12: Variation of the extrapolated contact modulus with the substrate modulus for (a) a 1μm thick coating with E_c=600GPa and (b) a 150nm coatings with E_c=140GPa. The extrapolation increasingly underestimates the true modulus as the coating thickness is reduced.

Figure 13: Variation of contact modulus with contact radius determined by two different methods. The contact radius determined from the contact area is more accurate as this takes into consideration the tip end shape whereas the contact radius determined from the contact depth assumes an ideal tip.

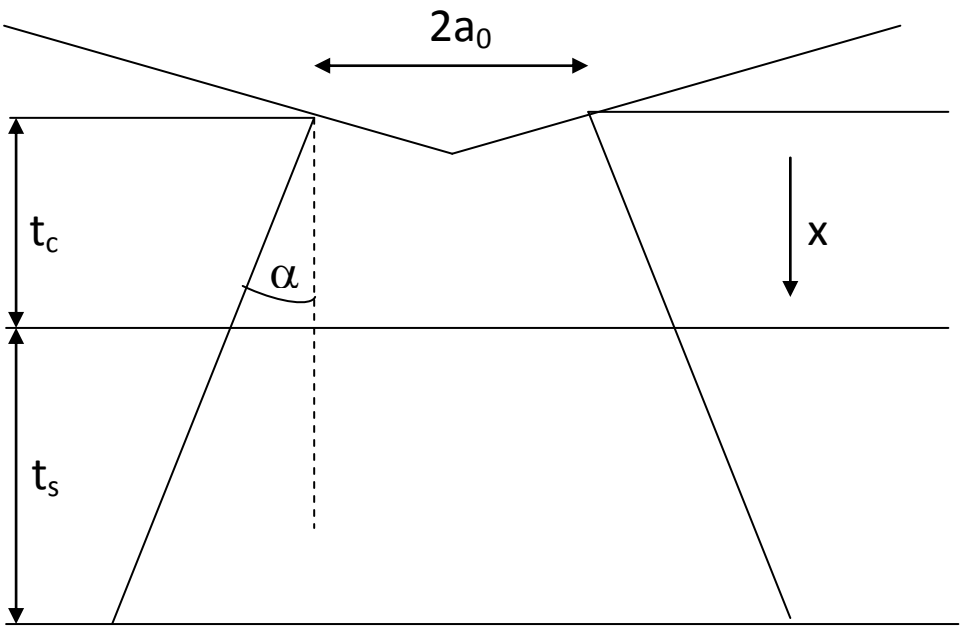

Figure 1: Cross sectional view of model geometry.

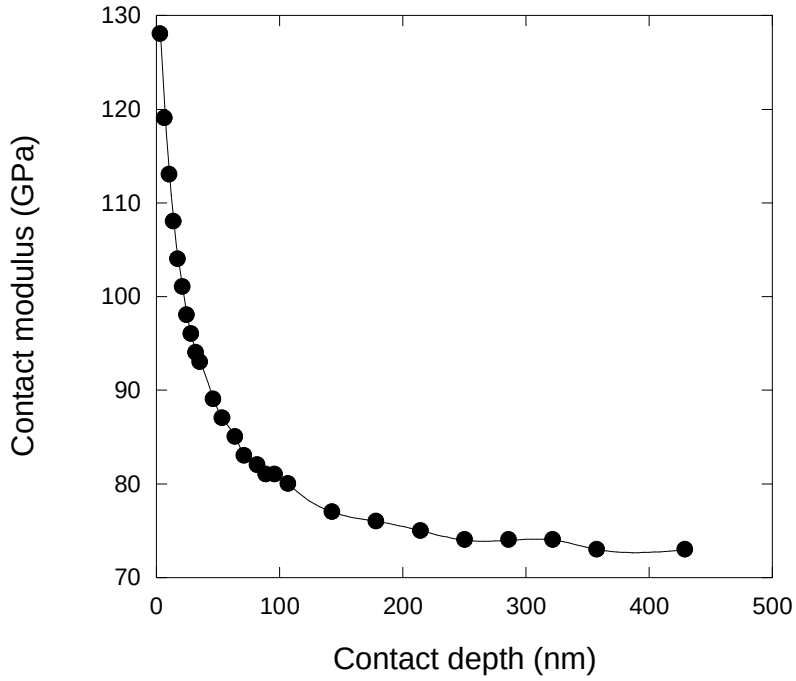

Figure 2: Variation of E with contact depth for a 150nm stiff coating (E=140GPa) on glass (E=70GPa).

(a)

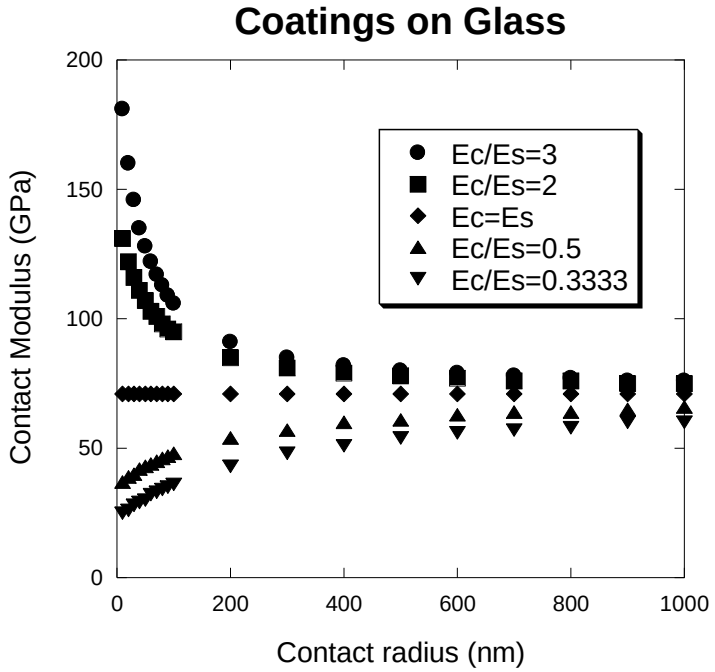

(b)

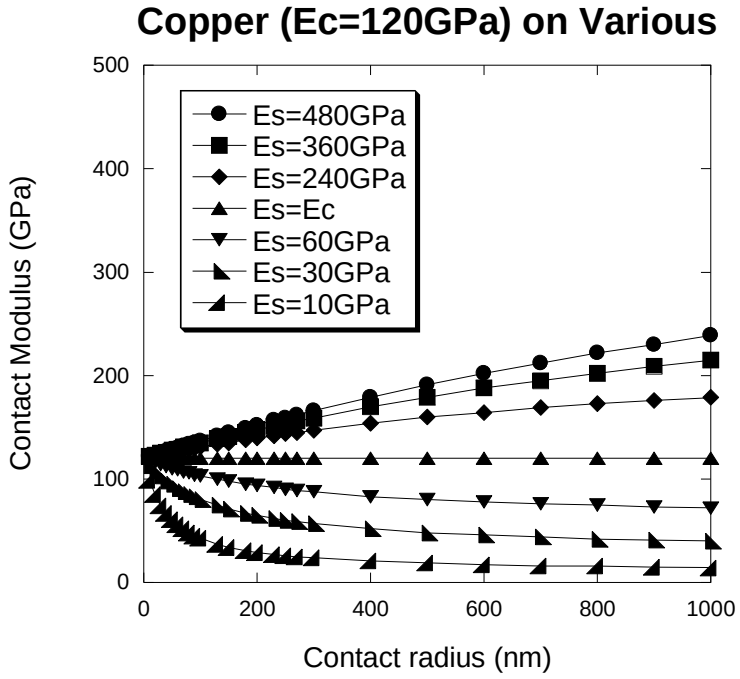

Figure 3: (a) Variation of E with contact radius for 150nm coatings with a range of elastic moduli on glass (E=70GPa). (b) Variation of E with contact radius for 800nm copper (Ec=120GPa) on various substrates.

(a)

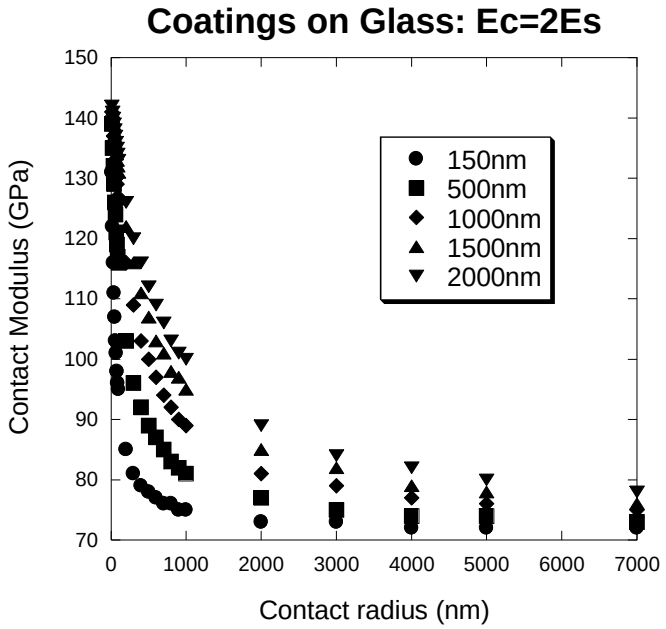

(b)

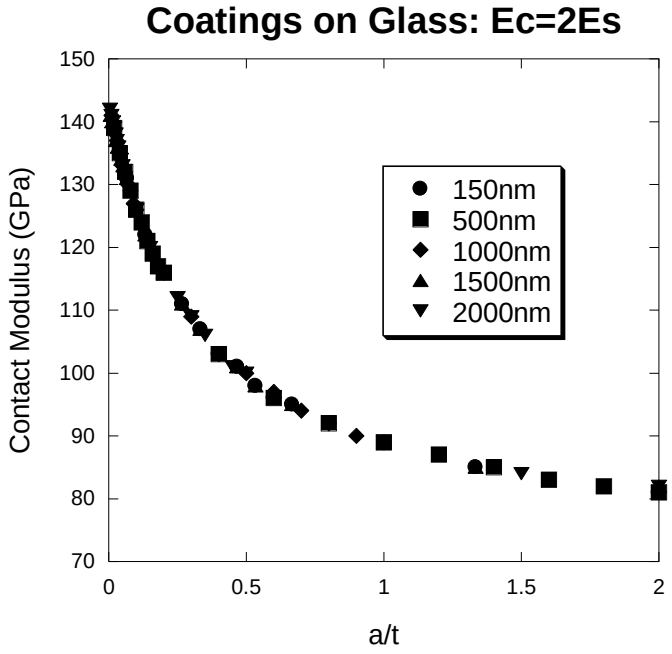

Figure 4 Variation of E with (a) contact radius, a and (b) a/t for a stiff coating (E=140GPa) on glass (E=70GPa).

(a)

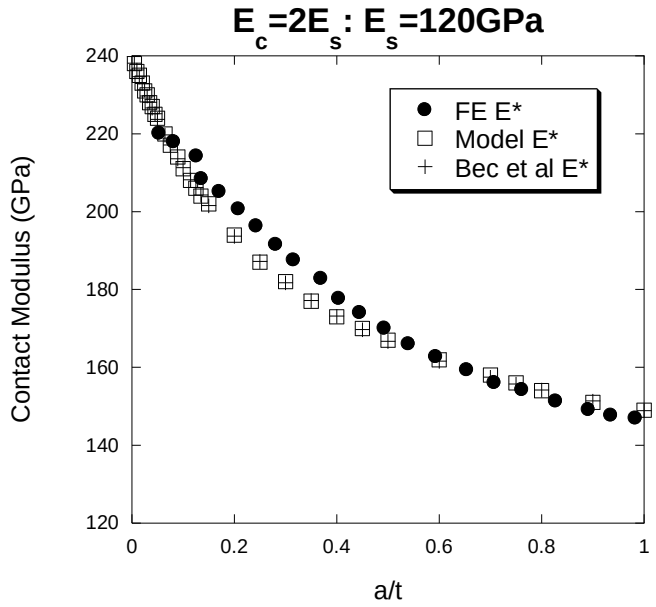

(b)

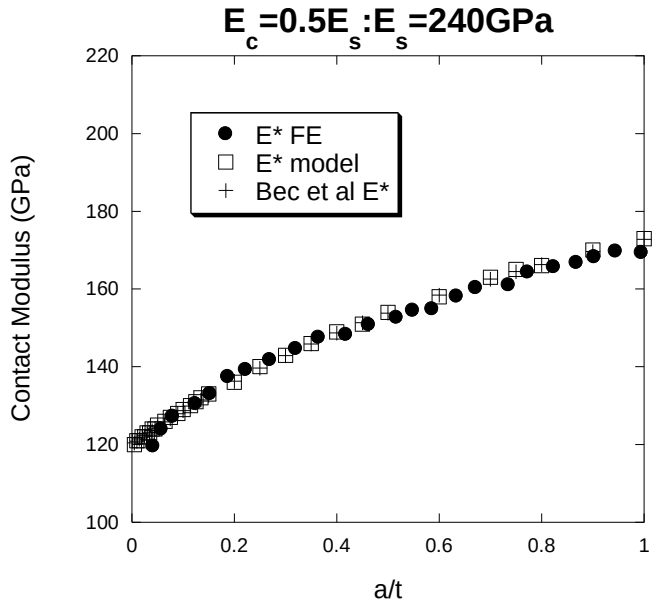

Figure 5: Comparison of model and FE predictions for coatings on different substrates, (a) $E_c=2E_s$ (E_s=120GPa) and (b) $E_c=0.5E_s$ (E_c=120GPa). The predictions from the model developed here and those from the model developed by Bec et al [9] are almost identical and match the FE data very well.

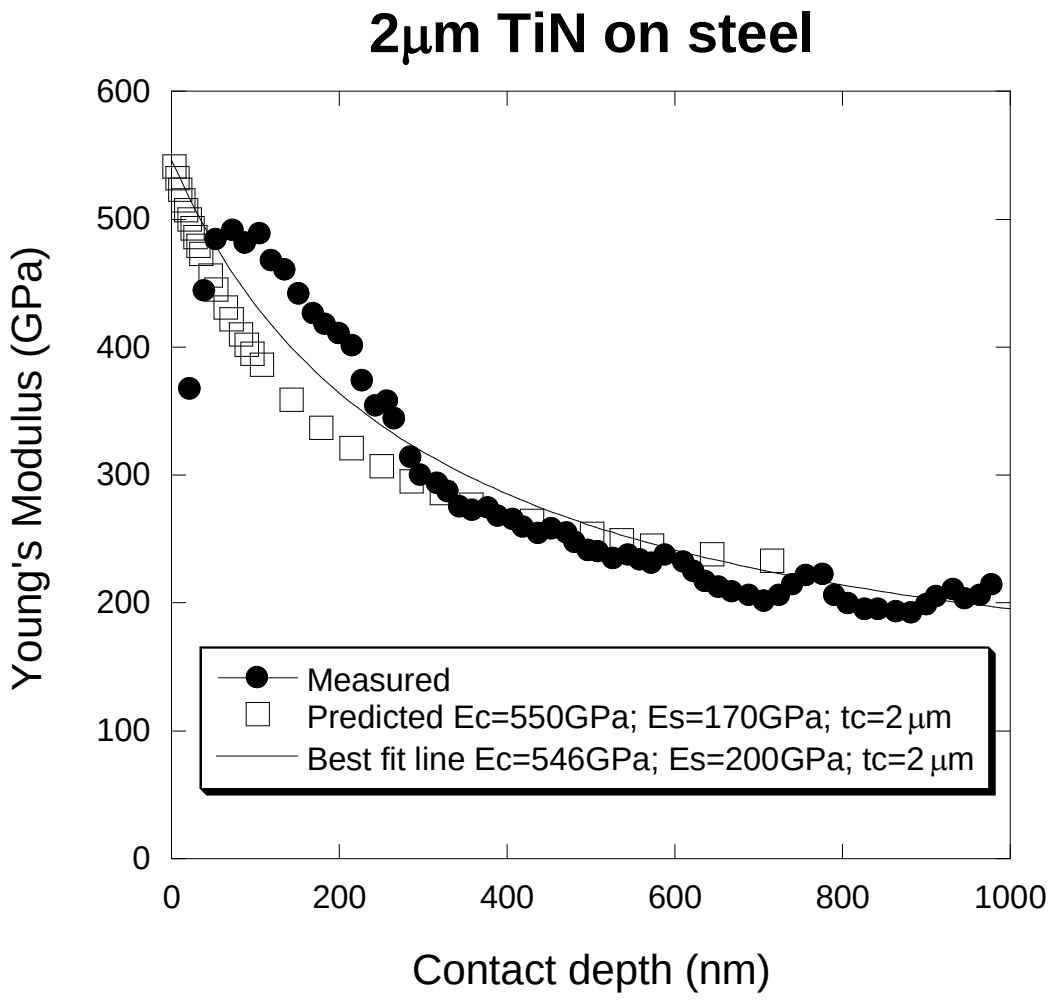

Figure 6: Young's modulus of TiN on stainless steel (Ra=30nm). Predictions from equation (15) using measured stiffness data and thicknesses are compared to experimental data and a fit of equation (15) to the experimental data. Coating properties are very consistent in both cases.

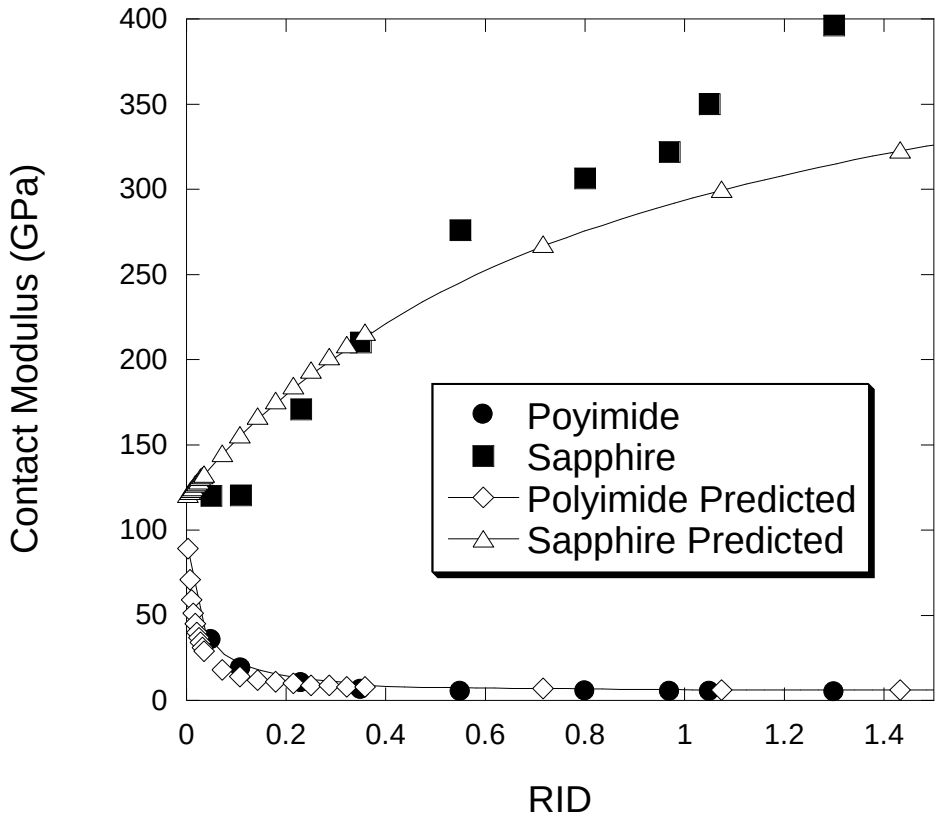

Figure 7 Contact modulus of 1μm copper on sapphire (Ra=5nm) and polyimide (Ra=20nm) as a function of contact scale.

(a)

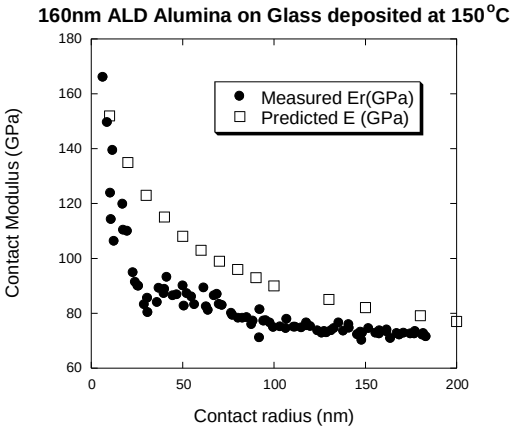

(b)

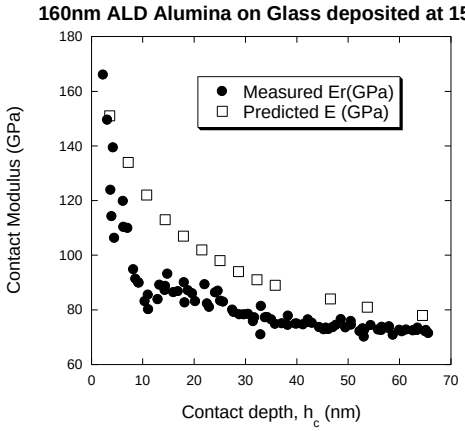

(c)

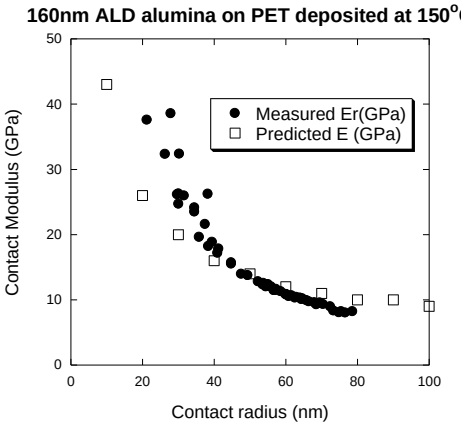

(d)

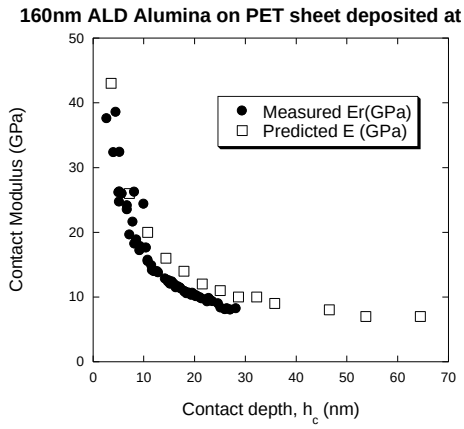

Figure 8 Contact modulus vs contact radius (a), (c) and contact depth (b), (d) for ALD alumina on glass (Ra~0.5nm) and PET (Ra~0.4nm) deposited at (a), (b) 80°C and (c), (d) 150°C. Coating properties determined in (a) and (b) are used for the predictions in (c) and (d).

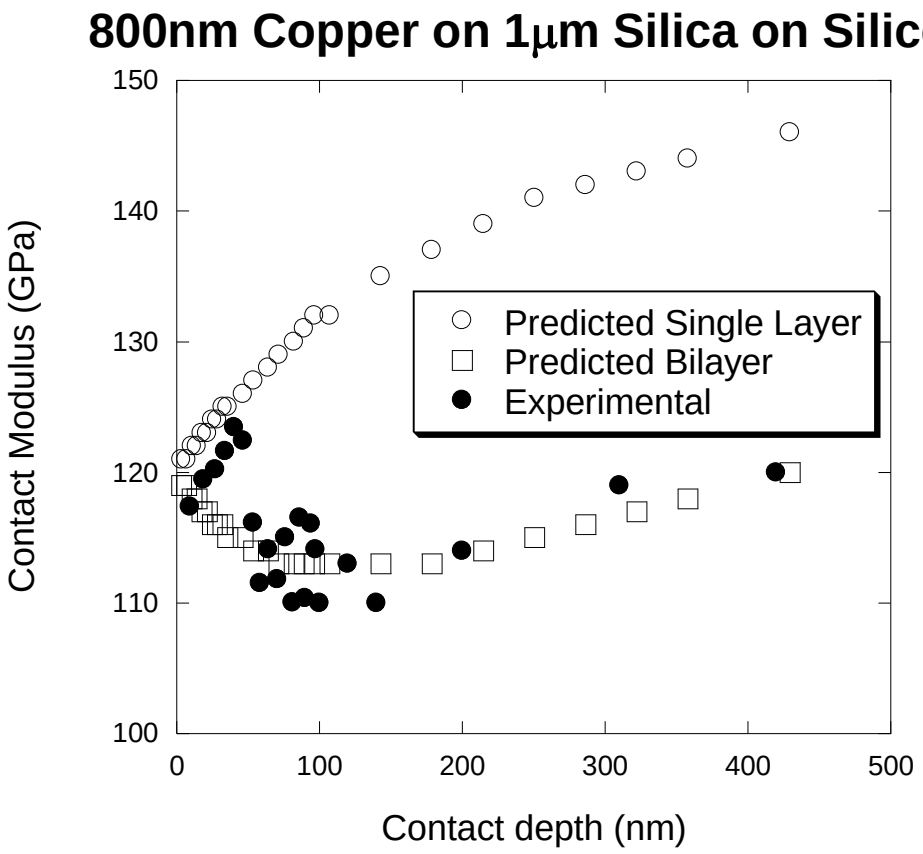

Figure 9 Contact modulus vs contact depth for 800nm copper on silicon (Ra=0.2nm) with a 1 micron silica intermediate layer. Predicted behaviour with and without the silica layer shows the importance of the silica in controlling behaviour.

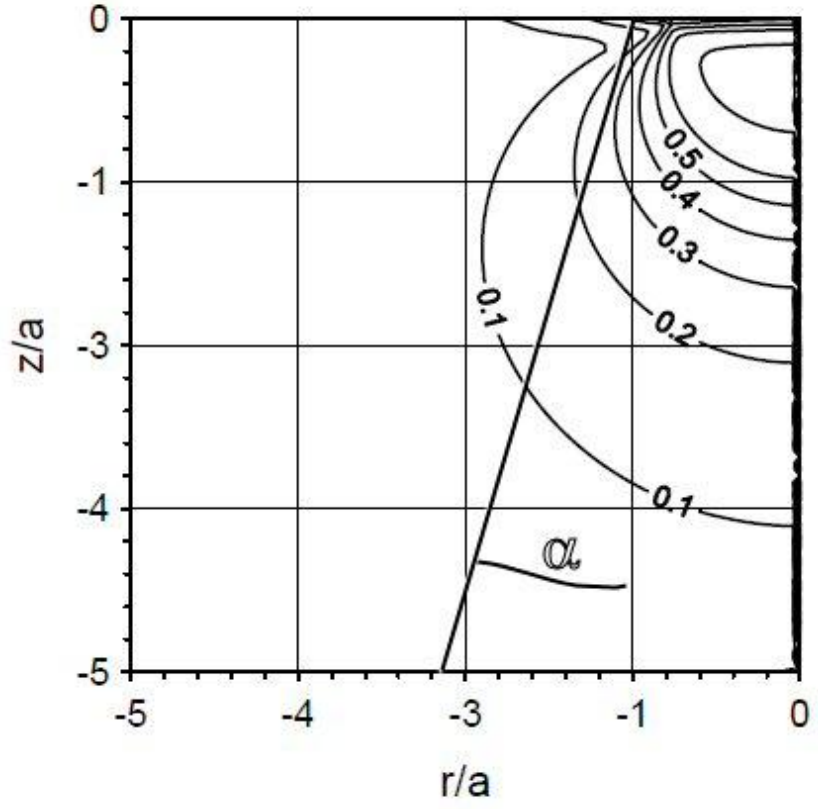

Figure 10 Comparison of the truncated cone geometry with the stress field under a conical indenter.

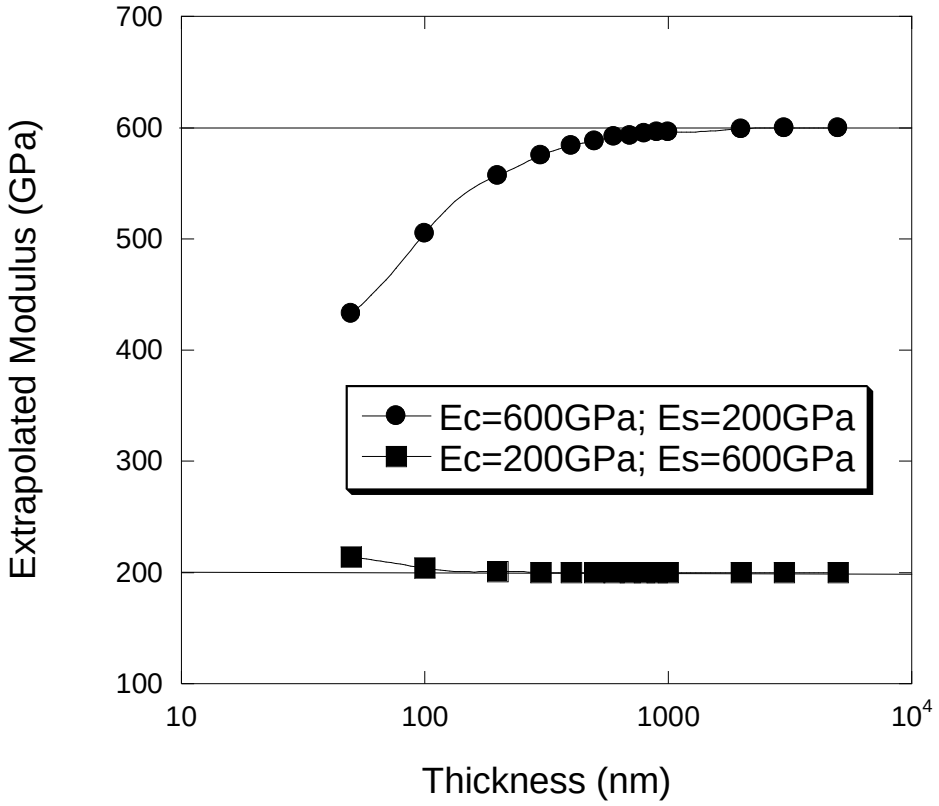

Figure 11: Variation of ratio of extrapolated contact modulus with coating thickness for two different coating/substrate compliance ratios. The stiff coating only gives accurate data when its thickness is greater than 1μm whereas accurate values for the contact modulus of the compliant coating can be determined down to a thickness of 100nm.

(a)

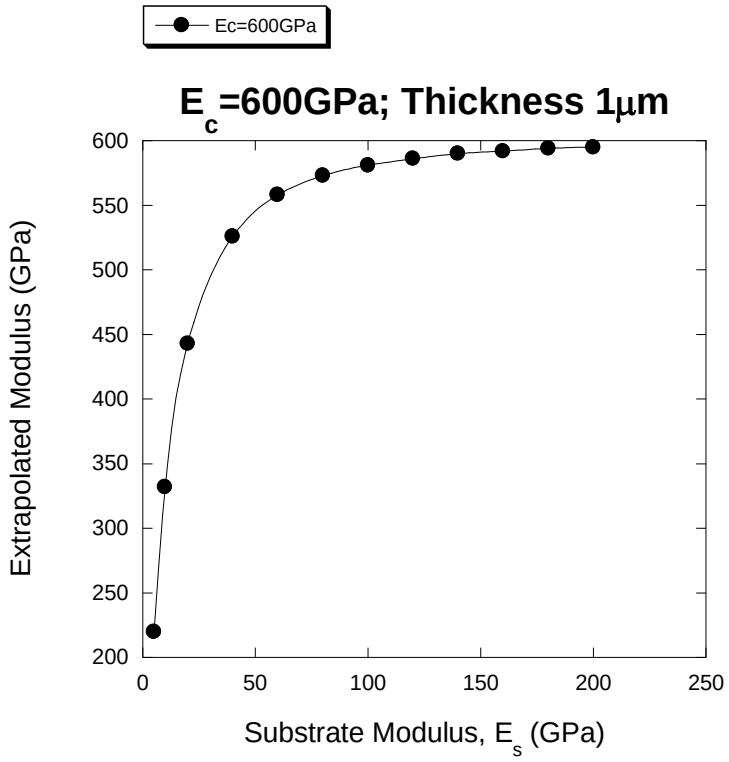

(b)

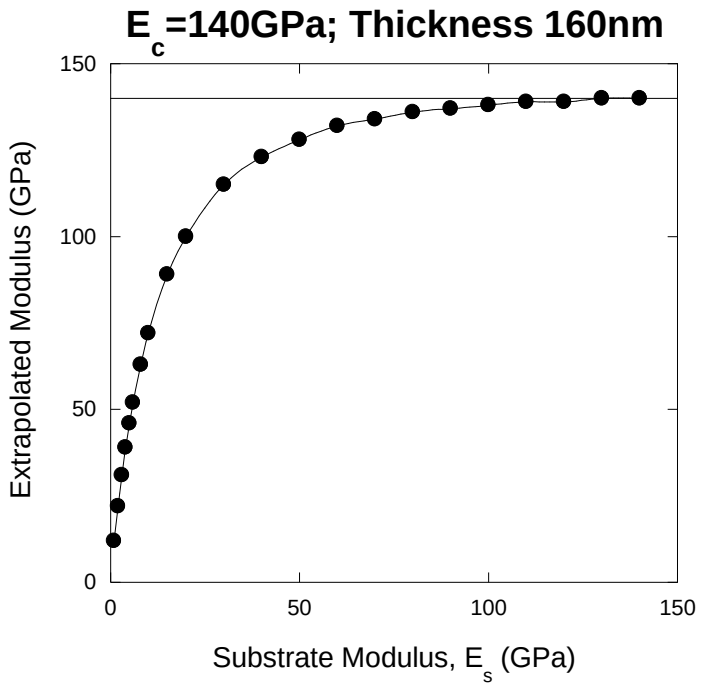

Figure 12: Variation of the extrapolated contact modulus with the substrate modulus for (a) a 1μm thick coating with E_c=600GPa and (b) a 150nm coatings with E_c=140GPa. The extrapolation increasingly underestimates the true modulus as the coating thickness is reduced.

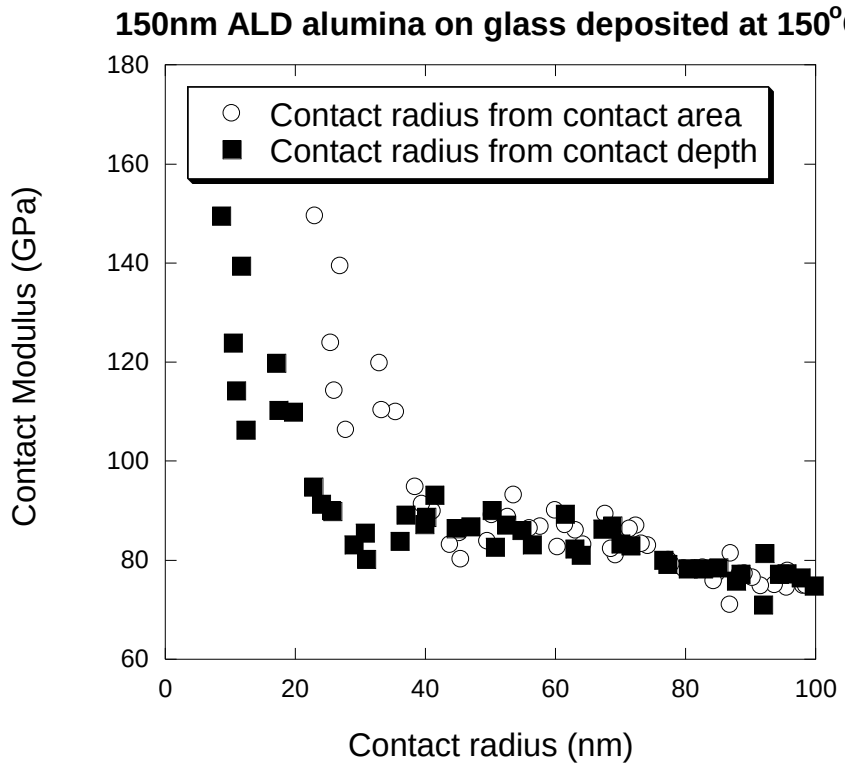

Figure 13: Variation of contact modulus with contact radius determined by two different methods. The contact radius determined from the contact area is more accurate as this takes into consideration the tip end shape whereas the contact radius determined from the contact depth assumes an ideal tip.